Chinese Journal of Polymer Science Vol. 33, No. 2, (2015), 301–317

Chinese Journal of Polymer Science

Synthesis and Characterization of Heterocyclic Functionalized Polymers by Click Reaction: Preparation of Magnetic Nanocomposites and Studies on Their Thermal, Mechanical, Photophysical and Metal Ions Removal Properties

Mousa Ghaemy*, Sahar Shabzendedar and Mehdi Taghavi
Polymer Chemistry Research Laboratory, Department of Chemistry, University of Mazandaran, Babolsar, 47416-95447, I.R. Iran

Abstract This work reports synthesis and characterization of heterocyclic functionalized polymers, poly(triazole-ether-imidazole)s (PTAEI), from a dialkyne-terminated compound, 3-(4,5-bis(4-(propargyloxy)phenyl)-1H-imidazol-2-yl)-9-ethyl-9H-carbazole, by using click reaction. PTAEIs were characterized and their properties such as solubility, thermal, mechanical, photophysical and metal ions adsorption were investigated. These polymers had weight average molar masses (M_w) in the range of 19100–26700 g/mol, exhibited excellent solubility in polar aprotic solvents and formed low-colored flexible thin films by solution casting method. They exhibited good thermal stability with glass transition temperatures (T_g) between 160 °C and 211 °C and 10% weight loss temperatures ($T_{10\%}$) in the range of 308–426 °C. Nanocomposites of PTAEIs with epoxide-terminated Fe_3O_4 showed that strong interfacial interaction between inorganic particles and the polymer matrix contributed to the enhanced thermal and mechanical properties. The photoluminescence intensity of the PTAEIs increased and the spectra red shifted with increasing Fe_3O_4 content. The PTAEIs and nanocomposites were tested for their extraction capability of metal ions from aqueous solutions either individually or in the mixture.

Keywords: Click chemistry; Heterocylic polymer; Poly(triazole-ether-imidazole); Magnetic nanocomposite; Metal ion removal.

INTRODUCTION

Reports on click chemistry are mostly on the Cu(I)-catalyzed Huisgen 1,3-dipolar cycloaddition reaction using azides as dipoles. This reaction gained a boost of interest after the copper-catalyzed version was introduced by Meldal and coworkers[1] and by Sharpless and coworkers[2] in 2002. Several reviews have developed applications of the triazole chemistry in many areas[3–5], and fundamental and mechanistic aspects of the copper catalyzed azide/alkyne cycloaddition were fully described[6]. The overall reaction is a cycloaddition of an alkyne and an organic azide to give a five-membered 1,2,3-triazole.

Many research efforts have been dedicated to design and produce novel polymers with improved solubility and processability by incorporating new chemical functionalities especially heterocyclic ring in the polymer backbone[7–11]. In this regard, the presence of heterocyclic ring such as imidazole, triazole or carbazole in the polymer chains[12–14], and their properties such as photoconductivity[15–17], interaction with metals[18, 19] and fluorescent on-off switchable chemosensors[20–22] were reported. However, the collective incorporation of heterocyclic rings in high performance polymer chains and their suitability in respect of thermal, solubility, mechanical and photophysical properties has not been overcome yet.

* Corresponding author: Mousa Ghaemy, E-mail: ghaemy@umz.ac.ir
Received April 23, 2014; Revised June 18, 2014; Accepted July 2, 2014
doi: 10.1007/s10118-015-1583-5

The combination of organic and inorganic components is expected to provide remarkable and complementary properties, which cannot be obtained with a single material[23–25]. Compared to composites containing larger dispersed particles, nanocomposites have the advantage of achieving the optimal properties at relatively low filler contents, resulting in a lower density and better surface smoothness and transparency. In recent years, variety of nanomaterials has been investigated for their tendency towards the removal of toxic metals from aqueous solution. Among many methods, adsorption was recognized as an effective and economic method for the removal of toxic metal ions from waste waters[26–31].

As a part of our continuing efforts to prepare novel high performance and processible functionalized polymers with unique properties, a new dialkyne-terminated aromatic heterocyclic compound with flexible ether linkages was designed, synthesized, characterized and used for preparation of poly(triazole-ether-imidazole)s (PTAEI)s by click reaction. These functionalized aromatic polymers were expected to show satisfactorily the required properties. The tertiary amines in the polymer chains were used in preparation of nanocomposites with the epoxide-functionalized magnetic Fe_3O_4 nanoparticles and also as the adsorbing sites of metal ions. The magnetic nanocomposite was separated easily from water by using an external magnet. PTAEIs were characterized with FTIR, H-NMR, and GPC, and nanocomposites with FTIR, XRD, SEM, AFM, TEM, and VSM. The properties of PTAEIs and nanocomposites such as solubility, thermal properties, fluorescence emission, and adsorption of Cr^{3+}, Pb^{2+}, Cd^{2+}, Sn^{2+}, Cu^{2+} and Hg^{2+} ions were investigated.

EXPERIMENTAL

Materials

All chemicals were purchased from Fluka and Merck Chemical Co. (Germany). Ammonium acetate, anhydrous potassium carbonate, sodium azide, sodium ascorbate, copper(II) sulfate pentahydrate, propargyl bromide and 3-glycidyloxypropyl trimethoxy silane (GPTES) were used as received. *N*,*N*-Dimethylformamide (DMF) were purified by distillation under reduced pressure over calcium hydride and stored over 4 Å molecular sieves.

Measurements

Proton and carbon nuclear magnetic resonance (^{1}H-NMR and ^{13}C-NMR) spectra were recorded on a 400 MHz and a 100 MHz instruments, respectively, Bruker Avance DRX Instrument (Germany) using DMSO-d_6 as solvent and tetramethyl silane as an internal standard. FTIR spectra were recorded using a Bruker Tensor 27 spectrometer on KBr pellets over the range of 400–4000 cm^{-1}. Elemental analyses were performed by a CHN-600 Leco elemental analyzer. Melting point was measured with a Barnstead Electrothermal Engineering LTD 9200 apparatus. Quantitative solubility was determined using 0.05 g of a polymer in 0.5 mL of solvent. Gel permeation chromatography (GPC) measurements were conducted at 30 °C with a Perkin-Elmer instrument equipped with a differential refractometer detector. The columns used were packed with a polystyrene/divinylbenzene copolymer (PL gel MIXED-B from Polymer Laboratories) with DMF as fluent at a flow rate of 1 mL/min. Monodisperse polystyrene standards were used for calibration of GPC. Thermogravimetric analysis (TGA) was performed with the DuPont Instruments (TGA 951) analyzer at 10 K/min under N_2 (20 cm^3/min) and in air in temperature range of 30–650 °C. Differential scanning calorimeter (DSC) was recorded on a Perkin Elmer Pyres 6 DSC under N_2 (20 cm^3/min) at 10 K/min. T_g values were read at the middle of the transition in heat capacity and were taken from the second heating scan after cooling from 350 °C at a cooling rate of 20 K/min. Ultraviolet-visible and fluorescence emission spectra were recorded on a Cecil 5503 (Cecil Instruments, Cambridge, UK) and Perkin-Elmer LS-3B spectrophotometers (Norwalk, CT, USA) (slit width = 2 nm), respectively, using a dilute polymer solution (0.20 g/dL) in DMSO. To prepare crack-free and homogeneous thin films for the measurement of optical properties, solutions were made by dissolving about 0.5 g polymer in 5 mL DMF to afford an approximate 10 wt% solution. The homogeneous solution was poured into a 9 cm-diameter glass culture dish, heated under vacuum at 50 °C for 2 h, 100 °C for 5 h, and 150 °C for 3 h to evaporate the solvent slowly. Polymer films were self-stripped off from the glass surface by soaking in water. The polymer films were further dried in vacuum oven at 170 °C for 10 h. X-ray powder diffraction

patterns were recorded by an X-ray diffractometer (GBC MMA instrument) with Be-filtered CuKα (0.15418 nm) operating at 35.4 kV and 28 mA. The 2θ scanning range was set between 4° and 50° at a scan rate of 0.05 (°)/s. Atomic force microscopic (AFM) Easy Scan 2 Flex AFM (Swiss Co), was used to investigate the surface phase and topography of the nanocomposites. FE-SEM was recorded on a Hitachi S4160 instrument. Magnetic properties of nanoparticles were measured at room temperature with a vibrating sample magnetometer (VSM) made by Daghigh Kavir Corporation (Iran). Branson S3200 (50 kHz, 150 W) ultrasonic bath was used for better dispersion of nanoparticles. To determine the tensile properties of the polymers, strips (5 mm in width and 30 mm in length) were cut from polymer films of 30–50 μm thickness on a MTS Criterion™ Universal Test Systems at 20 °C. Mechanical clamps were used and an extension rate of 5 mm/min was applied using a gauge length of 10 mm. At least six samples were tested for each polymer, and the average values are reported. For the moisture absorption measurement, 200 mg PTAEI or nanocomposite powder was dried at 120 °C for 8 h and then was placed in an open space with a relative humidity of 80%. The samples were weighed periodically over the course of 48 h. The solid-liquid extraction of Cr^{3+}, Pb^{2+}, Cd^{2+}, Sn^{2+}, Cu^{2+} and Hg^{2+} as their nitrate salts was carried out at pH = 7–8. Approximately 50 mg of the appropriate polymer powder was shaken with 50 mL of an aqueous solution of the metal salt for a week at 25 °C (equilibrium was assessed in less than three days). The initial concentration of salts was 20 mg/L. After filtration, the concentration of each metal cation in the liquid phase was determined by atomic absorption (BRAIC WFX-130 AA), and direct information regarding the extraction percentages of metal ions by polymers was obtained by using a calibration curve made from standard solutions of 0.5×10^{-4}, 1×10^{-4}, and 2×10^{-4} mol/L for each metal salts.

Monomer Synthesis

The procedures for synthesis of starting materials, diazides, monomer and PTAEIs are shown in Scheme 1.

*Synthesis of 4,4'-dihydroxy benzil (**1**)*

4,4'-Dihydroxy benzil was synthesized according to the procedure given in the literature[31].

*Synthesis of 4,4'-dipropargyloxy benzil (**2**)*

In a 100 mL round-bottomed two-necked flask equipped with a condenser, a magnetic stir bar and a nitrogen gas inlet tube, a mixture of 4,4'-dihydroxy benzil (2 g, 8.3 mmol), propargyl bromide (2.2 mL, 80% *W*/*V*, 15 mmol) and 2.76 g (20 mmol) anhydrous potassium carbonate in 10 mL dry acetonitrile was refluxed at 90 °C for 12 h. After completion of the reaction (as witnessed by TLC test), the solution was cooled to room temperature, filtered to remove potassium carbonate, solvent evaporated under reduced pressure and the obtained solid was dried in a vacuum oven. Yield was 96% (2.52 g) and m.p. 137–139 °C. FTIR (KBr, cm^{-1}): 3231 (≡CH stretching), 3044 (C−H aromatic stretching), 2923 (C−H aliphatic stretching), 2098 (C≡C), 1651 (C=O stretching), 1582 (C=C stretching), 1232 (C−O stretching). ^{1}H-NMR (400 MHz, DMSO-d_6, δ): 3.67 (t, 2H, ≡CH, J = 2.4 Hz), 4.96 (d, 4H, CH_2, J = 2.4 Hz), 7.19 (d, 4H, Ar−H, J = 8.0 Hz), 7.89 (d, 4H, Ar−H, J = 8.0 Hz).

*Synthesis of 3-(4,5-bis(4-(propargyloxy)phenyl)-1H-imidazol-2-yl)-9-ethyl-9H-carbazole (**3**)*

Into a 100 mL round-bottomed two-necked flask equipped with a condenser, a magnetic stirring bar and a nitrogen gas inlet tube, a mixture of 9-ethyl-carbazole-2-carbaldehyde (1.11 g, 5 mmol), compound **2** (1.58 g, 5 mmol), ammonium acetate (2.7 g, 35 mmol), and glacial acetic acid (25 mL) was refluxed for 14 h. Upon cooling, the yellow precipitate was filtered, washed with a mixture of ethanol/water (50/50, *V*/*V*) and dried in a vacuum oven at 80 °C. Yield was 91% (2.35 g) and m.p. 199–200 °C. FTIR (KBr) at cm^{-1}: 3473 (NH, imidazole ring), 3234 (≡CH stretching), 3011 (C−H aromatic stretching), 2942 (C−H aliphatic stretching), 2125 (C≡C), 1604 (C=N), 1517 (C=C), 1271 (C−N), 1249 (C−O−C). ^{1}H-NMR (400 MHz, DMSO-d_6, δ): 1.35 (t, 3H, CH_3, J = 6.8 Hz), 3.62 (s, 2H, ≡CH), 4.48 (q, 2H, −CH_2), 4.84 (s, 4H, −CH_2), 7.00 (s, 4H, Ar−H), 7.25 (t, 1H, Ar−H, J = 7.2 Hz), 7.49 (m, 5H, Ar−H), 7.64 (d, 1H, Ar−H, J = 8.4 Hz), 7.71 (d, 1H, Ar−H, J = 8.8 Hz), 8.17 (d, 1H, Ar−H, J = 7.6 Hz), 8.21 (dd, 1H, Ar−H, J_1 = 8.2 Hz, J_2 = 1.2 Hz), 8.83 (d, 1H, Ar−H, J = 1.2 Hz), 12.49 (s, 1H, N−H). ^{13}C-NMR (100 MHz, DMSO-d_6, δ): 1 (14.26), 2 (37.56), 3 (55.88), 4 (78.76), 5

(79.79), 6 (109.67), 7 (109.84), 8 (115.61), 9 (116.58), 10 (117.44), 11 (119.55), 12 (120.71), 13 (122.16), 14 (122.22), 15 (122.67), 16 (122.74), 17 (123.94), 18 (126.46), 19 (129.41), 20 (129.45), 21 (132.74), 22 (139.81), 23 (140.47), 24 (144.80), 25 (146.07) , 26 (150.10), 27 (156.83), 28 (156.86). DEPT Technique (135 MHz, DMSO-d_6): δ 1 (14.26), 2 (37.56), 3 (55.88), 4 (78.77), 5 (109.67), 6 (109.84), 7 (115.61), 8 (116.59), 9 (117.44), 10 (119.55), 11 (120.71), 12 (123.94), 13 (126.46), 14 (129.41), 15 (129.45). Elemental analysis calculated for ($C_{35}H_{27}N_3O_2$): C, 80.61%; H, 5.18%; N, 8.06%. Found: C, 79.96%; H, 5.39%; N, 8.02%.

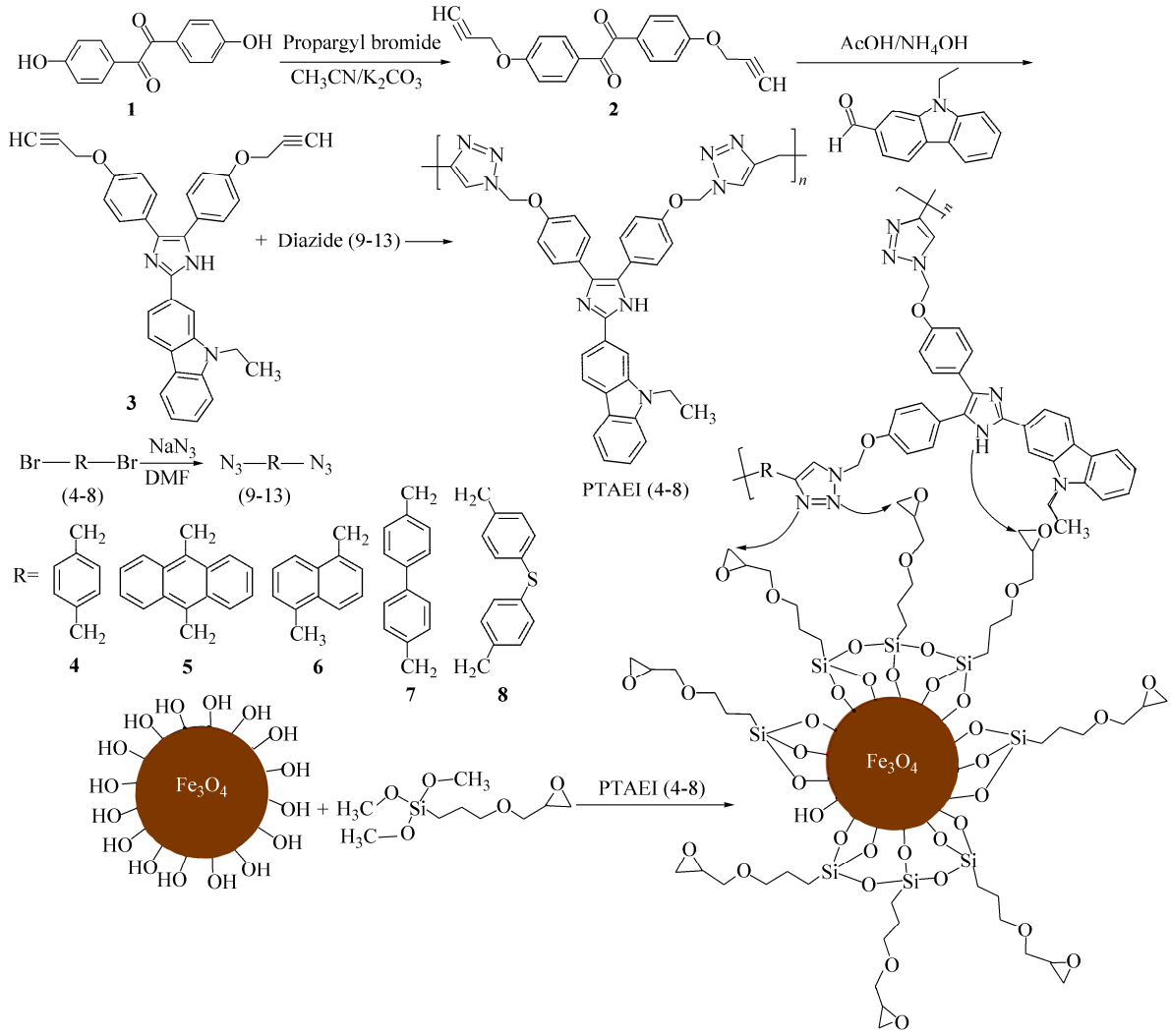

Scheme 1 Illustration of synthesis of compound **3**, click reaction and nanocomposite intercalation

*Synthesis of 1,4-bis(bromomethyl)benzene (**4**)*

Compound **4** was synthesized according to the procedure in the literature[32]. Yield was 61% (48 g) and m.p. 142–144 °C. FTIR (KBr) at cm^{-1}: 3056 (C—H aromatic stretching), 2987 (C—H aliphatic stretching), 1667 (C=C), 1265 (CH_2—Br bending), 705 (C—Br stretching). ^{1}H-NMR (400 MHz, $CDCl_3$, δ): 4.50 (s, 4H, CH_2), 7.39 (s, 4H, Ar—H).

*Synthesis of 9,10-bis(bromomethyl)anthracene (**5**)*

Compound **5** was synthesized according to the procedure in the literature[33]. Yield was 81% (6.62 g) and m.p. 300–301 °C. FTIR (KBr) at cm^{-1}: 3059 (C—H aromatic stretching), 2989 (C—H aliphatic stretching), 1666

(C=C), 1266 (CH_2−Br bending), 703 (C−Br stretching). ^{1}H-NMR (400 MHz, $CDCl_3$, δ): 5.54 (s, 4H, CH_2), 7.69–7.71 (m, 4H, Ar−H), 8.39–8.41 (m, 4H, Ar−H).

*Synthesis of 1,5-bis(bromomethyl)naphthalene (**6**)*

Compound **6** was synthesized according to the procedure in the literature[33]. Yield was 67% (6.7 g) and m.p. 212–214 °C. FTIR (KBr) at cm^{-1}: 3056 (C−H aromatic stretching), 2986 (C−H aliphatic stretching), 1666 (C=C), 1266 (CH_2−Br bending), 700 (C−Br stretching). ^{1}H-NMR ($CDCl_3$, 400 MHz, δ): 4.96 (s, 4 H, CH_2), 7.56 (2H, d, J = 8.0 Hz), 7.69 (2H, d, Ar−H, J = 7.4 Hz), 8.18 (2H, d, Ar−H, J = 8.4 Hz).

*Synthesis of 4,4'-bis(bromomethyl)- 1,1'-biphenyl (**7**)*

Compound **7** was synthesized according to the procedure in the literature[33]. Yield 5.62 g (51%) product with m.p. 169–171 °C. FTIR (KBr) at cm^{-1}: 3055 (C−H aromatic stretching), 2987 (C−H aliphatic stretching), 1668 (C=C), 1265 (CH_2−Br bending), 706 (C−Br stretching). ^{1}H-NMR (400 MHz, $CDCl_3$, δ): 4.58 (s, 4 H, CH_2), 7.49 (d, 4H, Ar−H, J = 8.4), 7.59 (d, 4 H, Ar−H, J = 8.4).

*Synthesis of bis(4-(bromomethyl)phenyl)sulfide (**8**)*

Compound **8** was synthesized according to the procedure in the literature[33]. Yield was 77% and m.p. 129–131 °C. FTIR (KBr) at cm^{-1}: 3055 (C−H aromatic stretching), 2987 (C−H aliphatic stretching), 1665 (C=C), 1266 (CH_2−Br bending), 701 (C−Br stretching). ^{1}H-NMR (400 MHz, $CDCl_3$, δ): 4.49 (s, 4H, CH_2), 7.31–7.37 (m, 8H, Ar−H).

*Synthesis of 1,4-bis(azidomethyl)benzene (**9**)*

A solution of **6** mmol 1,4-bis(bromomethyl)benzene and 10 mmol NaN_3 in 30 mL DMF was stirred at room temperature for 24 h, then poured into 50 mL water and extracted with diethyl ether (3 × 20 mL). The combined organic phases were washed with water, brine, dried over anhydride $MgSO_4$, evaporated carefully and the pure compound was isolated as a white solid. Yield was 96% (5.76 mmol) and m.p. 27–29 °C. FTIR (KBr) at cm^{-1}: 3059 (C−H aromatic stretching), 2988 (C−H aliphatic stretching), 2096 (N_3), 1663 (C=C), 1265 (CH_2−Br bending), 701 (C−Br stretching). ^{1}H-NMR (400 MHz, $CDCl_3$, δ): 4.38 (s, 4H, CH_2), 7.37 (s, 4H, Ar−H).

All diazide compounds (**9**–**13**) were prepared according to the above general procedure.

*Synthesis of 9,10-bis(azidomethyl)anthracene (**10**)*

Yellow crystal, yield = 93% and m.p. = 187–189 °C. FTIR (KBr) at cm^{-1}: 3055 (C−H aromatic stretching), 2987 (C−H aliphatic stretching), 2097 (N_3), 1665 (C=C), 1265 (CH_2−Br bending), 706 (C−Br stretching). ^{1}H-NMR (400 MHz, $CDCl_3$, δ): 5.39 (s, 4H, CH_2), 7.66–7.69 (m, 4H, Ar−H), 8.39–8.41 (m, 4H, Ar−H).

*Synthesis of 1,5-bis(azidomethyl)naphthalene (**11**)*

Light yellow powder, yield = 86% and m.p. = 39–41 °C. FTIR (KBr) at cm^{-1}: 3055 (C−H aromatic stretching), 2986 (C−H aliphatic stretching), 2101 (N_3), 1673 (C=C), 1265 (CH_2−Br bending), 701 (C−Br stretching). ^{1}H-NMR (400 MHz, $CDCl_3$, δ): 4.96 (s, 4 H, CH_2), 7.49 (dd, 2H, J = 7.8 Hz), 7.60 (d, 2H, J = 7.0 Hz), 8.09 (d, 2H, J = 8.2 Hz).

*Synthesis of 4,4'-bis(azidomethyl)-1,1'-biphenyl (**12**)*

White powder, yield = 92% and m.p. = 73–74 °C. FTIR (KBr) at cm^{-1}: 3054 (C−H aromatic stretching), 2985 (C−H aliphatic stretching), 2100 (N_3), 1666 (C=C), 1266 (CH_2−Br bending), 705 (C−Br stretching). ^{1}H-NMR (400 MHz, $CDCl_3$, δ): 4.41 (s, 4H, CH_2), 7.40 (d, 4H, Ar−H, J = 8.2 Hz), 7.61 (d, 4H, Ar−H, J = 8.2 Hz).

*Synthesis of bis(4-(azidomethyl)phenyl)sulfane (**13**)*

White powder, yield = 88% and m.p. = 20–21 °C. FTIR (KBr) at cm^{-1}: 3054 (C−H aromatic stretching), 2986 (C−H aliphatic stretching), 2100 (N_3), 1674 (C=C), 1265 (CH_2−Br bending), 703 (C−Br stretching). ^{1}H-NMR (400 MHz, $CDCl_3$, δ): 4.36 (s, 4H, CH_2), 7.28–7.30 (m, 4H, Ar−H), 7.36–7.38 (m, 4H, Ar−H).

Synthesis of PTAEIs

The following general procedure, as illustrated in Scheme 1, was used for preparation of PTAEIs from dipropargyl compound (**3**) and various diazides (**9**–**13**). In a 50 mL round-bottomed flask was added compound (**3**) (2 mmol), a diazide compound (2 mmol), DMF (5 mL), copper sulfate (0.09 mmol) and sodium ascorbate (0.18 mmol). The mixture was stirred at room temperature for 16–24 h and the resulting polymers were precipitated in 50 mL methanol. The precipitate was filtered and washed with hot water, and then was further purified by washing with refluxing methanol in a soxhelet apparatus for 1 day to remove the low molecular weight fractions.

PTAEI4: Yield = 86% and η_{inh} = 0.44 dL/g. FTIR (KBr disk) at cm^{-1}: 3198–3514 (NH imidazole), 3039 (C－H aromatic), 2933 (C－H aliphatic), 1614 (C＝N), 1513 (C＝C), 1225 (C－O). ^{1}H-NMR (400 MHz, DMSO-d_6, δ): 1.31 (t, 3H, CH_3, J = 6.8 Hz), 4.44 (q, 2H, CH_2, J = 6.8 Hz), 5.09 (s, 2H, CH_2－N), 5.14 (s, 2H, CH_2－N), 5.58 (s, 4H, CH_2－O), 6.95–7.67 (m, 16H, Ar－H), 8.18–8.20 (m, 2H, Ar－H), 8.26–8.30 (m, 2H, CH Triazole ring), 8.82 (S, 1H, Ar－H), 12.45 (s, 1H, NH Imidazole ring). Elemental analysis calculated for $(C_{43}H_{35}N_9O_2)_n$: C, 72.78%; H, 4.94%; N, 17.77% and found: C, 72.31%; H, 5.16%; N, 17.68%.

PTAEI5: Yield = 88% and η_{inh} = 0.46 dL/g. FTIR (KBr disk) at cm^{-1}: 3209–3526 (NH imidazole), 3033 (C－H aromatic), 2937 (C－H aliphatic), 1616 (C＝N), 1508 (C＝C), 1224 (C－O). ^{1}H-NMR (400 MHz, DMSO-d_6, δ): 1.33 (t, 3H, CH_3, J = 6.8 Hz), 4.46 (q, 2H, CH_2, J = 6.8 Hz), 4.84 (s, 4H, CH_2－N), 5.54 (s, 4H, CH_2－O), 6.72–7.69 (m, 16H, Ar－H), 8.23–8.27 (m, 2H, CH Triazole ring), 8.67–8.72 (m, 6H, Ar－H), 8.81 (s, 1H, Ar－H), 12.41 (s, 1H, NH Imidazole ring). Elemental analysis calculated for $(C_{51}H_{39}N_9O_2)_n$: C, 75.65%; H, 4.82%; N, 15.58% and found: C, 75.47%; H, 5.29%; N, 15.49%.

PTAEI6: Yield = 80% and η_{inh} = 0.55 dL/g. FTIR (KBr disk) at cm^{-1}: 3208–3501 (NH imidazole), 3036 (C－H aromatic), 2940 (C－H aliphatic), 1618 (C＝N), 1512 (C＝C), 1227 (C－O). ^{1}H-NMR (400 MHz, DMSO-d_6, δ): 1.33 (t, 3H, CH_3, J = 6.8 Hz), 4.47 (q, 2H, CH_2, J = 6.8 Hz), 5.11 (s, 2H, CH_2－N), 5.16 (s, 2H, CH_2－N), 5.61 (s, 4H, CH_2－O), 6.94–7.62 (m, 16H, Ar－H), 8.15–8.20 (m, 4H, Ar－H), 8.22–8.26 (m, 2H, CH Triazole ring), 8.83 (s, 1H, Ar－H), 12.45 (s, 1H, NH Imidazole ring). Elemental analysis calculated for $(C_{47}H_{37}N_9O_2)_n$: C, 74.31%; H, 4.87%; N, 16.60% and found: C, 73.98%; H, 5.08%; N, 16.51%.

PTAEI7: Yield = 83% and η_{inh} = 0.41 dL/g. FTIR (KBr disk) at cm^{-1}: 3197–3511 (NH imidazole), 3038 (C－H aromatic), 2932 (C－H aliphatic), 1609 (C＝N), 1511 (C＝C), 1223 (C－O). ^{1}H-NMR (400 MHz, DMSO-d_6, δ): 1.34 (t, 3H, CH_3, J = 6.8 Hz), 4.48 (q, 2H, CH_2, J = 6.8 Hz), 5.13 (s, 2H, CH_2－N), 5.17 (s, 2H, CH_2－N), 5.65 (s, 4H, CH_2－O), 6.94–7.72 (m, 20H, Ar－H), 8.16–8.22 (m, 2H, Ar－H), 8.28–8.32 (s, 2H, CH Triazole ring), 8.83 (s, 1H, Ar－H), 12.47 (s, 1H, NH Imidazole ring). Elemental analysis calculated for $(C_{49}H_{39}N_9O_2)_n$: C, 74.90%; H, 4.97%; N, 16.10% and found: C, 74.46%; H, 5.38%; N, 16.00%.

PTAEI8: Yield = 91% and η_{inh} = 0.59 dL/g. FTIR (KBr disk) at cm^{-1}: 3184–3508 (NH imidazole), 3046 (C－H aromatic), 2943 (C－H aliphatic), 1612 (C＝N), 1516 (C＝C), 1228 (C－O). ^{1}H-NMR (400 MHz, DMSO-d_6, δ): 1.31 (t, 3H, CH_3, J = 6.8 Hz), 4.45 (q, 2H, CH_2, J = 6.8 Hz), 5.10 (s, 2H, CH_2－N), 5.16 (s, 2H, CH_2－N), 5.59 (s, 4H, CH_2－O), 6.97–7.66 (m, 20H, Ar－H), 8.15–8.21 (m, 2H, Ar－H), 8.26–8.29 (m, 2H, CH Triazole ring), 8.82 (s, 1H, Ar－H), 12.45 (s, 1H, CH Imidazole ring). Elemental analysis calculated for $(C_{49}H_{39}N_9O_2S)_n$: C, 71.97%; H, 4.77%; N, 15.42% and found: C, 71.19%; H, 5.47%; N, 15.39%.

Preparation of Fe_3O_4 Nanoparticles

Fe_3O_4 was prepared by the conventional *co*-precipitation method[34]. Firstly, mixture of 5.2 g $FeCl_3$, 2.0 g $FeCl_2$ and 0.85 mL HCl (12 mol/L) was dissolved in 25 mL deionized water under N_2 protection. The resulting solution was added drop-wise into 250 mL of 1.5 mol/L NaOH solution under vigorous stirring. After the reaction, the obtained precipitate was separated from the reaction medium under the magnetic field and washed with deionized water and ethanol for several times. Finally, a portion of Fe_3O_4 was dispersed in ethanol with the concentration of 5 g/L.

Preparation of GPTES-Fe_3O_4 Nanoparticles

A suspension of 1 g Fe_3O_4 in 30 mL ethanol and deionized water (50/50, *V*/*V*) was sonicated in 150 W ultrasonic

water bath for 30 min. Then 1 g GPTES was added to this sonicated suspension solution and stirred at 80 °C for 4 h, and then left at room temperature for 24 h. Finally, the GPTES-Fe_3O_4 was separated from the mixture by the centrifugation and washed with ethanol for several times. Before the next step, the GPTES-Fe_3O_4 particles were dispersed in ethanol with the concentration of 1 g/L[34].

Preparation of GPTES-Fe_3O_4/PTAEI Nanocomposites

0.1 g of a PTAEI was dispersed in 20 mL dried DMAc and the solution was ultra sonicated for about 30 min in a 150 W water ultrasonic bath. Then a certain amount of GPTES-Fe_3O_4 (10 wt% and 30 wt% based on weight of PTAEI) was added to the resulting solution and the mixture was ultra sonicated for 30 min at 70 °C. After irradiation, the mixture was continuously stirred at 70 °C for 5 h under N_2 atmosphere. Then solvent was removed, and the obtained nanocomposite was dried in a vacuum oven at 80 °C for 24 h.

RESULTS AND DISCUSSION

Synthesis and Characterization of Monomer (3)

A dialkyl-terminated compound, 3-(4,5-bis(4-(propargyloxy)phenyl)-1H-imidazol-2-yl)-9-ethyl-9H-carbazole, was synthesized in three steps according to the synthetic route shown in Scheme 1. Condensation of 4,4'-dimethoxy benzil with aqueous HBr in glacial acetic acid afforded compound **1** which was converted into compound **2** by nucleophilic substitution reaction with propargyl bromide. In the FTIR spectrum of compound **2**, absorption band related to hydroxyl groups disappeared and new absorption bands were observed at 2300 cm^{-1} and 3200 cm^{-1} due to −C≡C− and C−H (connected to C≡C) stretching vibrations, respectively. ^{1}H-NMR spectrum of compound **2** showed two new signals at δ = 3.67 and 4.96 related to ≡C−H and CH_2 protons, respectively. The reaction between compound **2** and 9-ethyl-carbazole-2-carbaldehyde in ammonium acetate which is a well-known synthetic method for preparation of imidazole ring was used to synthesize the target monomer, compound **3**. The purity of all compounds was checked by thin-layer chromatography.

The structure of compound **3** was confirmed by elemental analysis, FTIR, and ^{1}H- and ^{13}C-NMR spectroscopy. ^{1}H-NMR spectrum of compound **3** in Fig. 1 shows N−H proton of imidazole at δ = 12.5, ≡C−H proton at δ = 3.61, −CH_3 protons at δ = 1.35 and −CH_2−C≡CH protons at δ = 4.86.

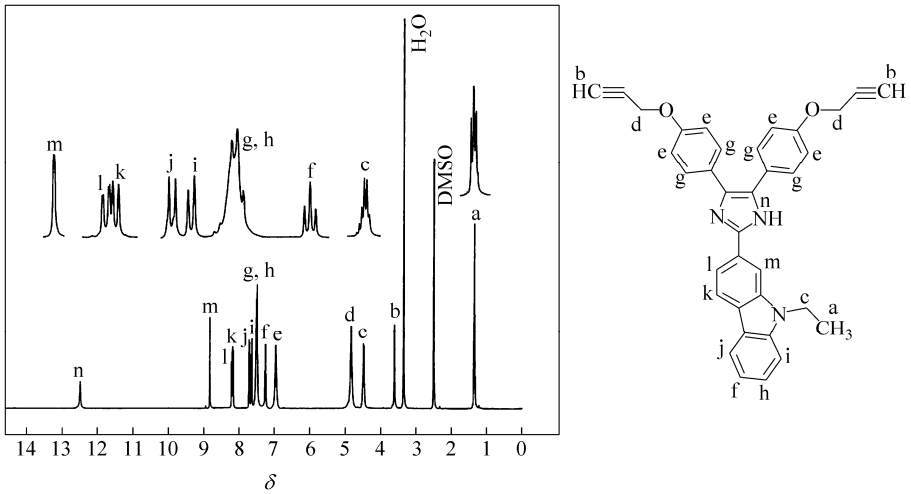

Fig. 1 ^{1}H-NMR spectrum of monomer (**3**) in DMSO-d_6

The appearance of N−H proton of imidazole at 3400 cm^{-1} in FTIR spectrum (Fig. 2), has confirmed the synthesis of compound (**3**) is successful. The ^{13}C-NMR spectrum of compound **3** in Fig. 3 shows 28 different carbon atoms. Also, new diazide compounds **9**–**13** were prepared *via* two-step synthesis. First, the corresponding dibromoethyl compounds **4**–**8** were prepared according to the procedures given in the literatures[32, 33].

Compounds **4**–**8** were then converted into diazide compounds **9**–**13** using sodium azide in DMF. The structure of diazide compounds was confirmed by FTIR and ^{1}H-NMR spectroscopy. The FTIR spectra of these compounds showed characteristic absorption band of azide at 2098 cm^{-1}.

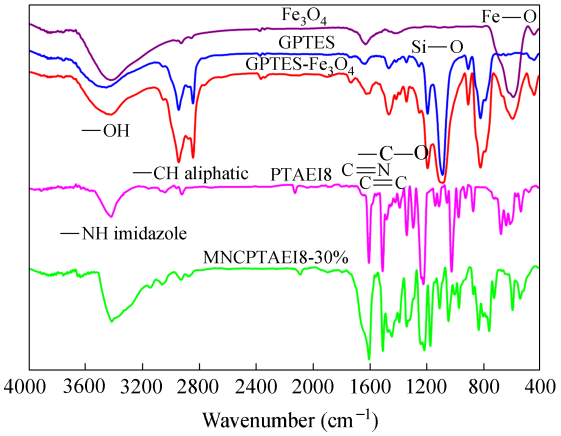

Fig. 2 FTIR spectra of Fe_3O_4, GPTES, GPTES-Fe_3O_4, PTAEI8 and MNCPTAEI8-30%

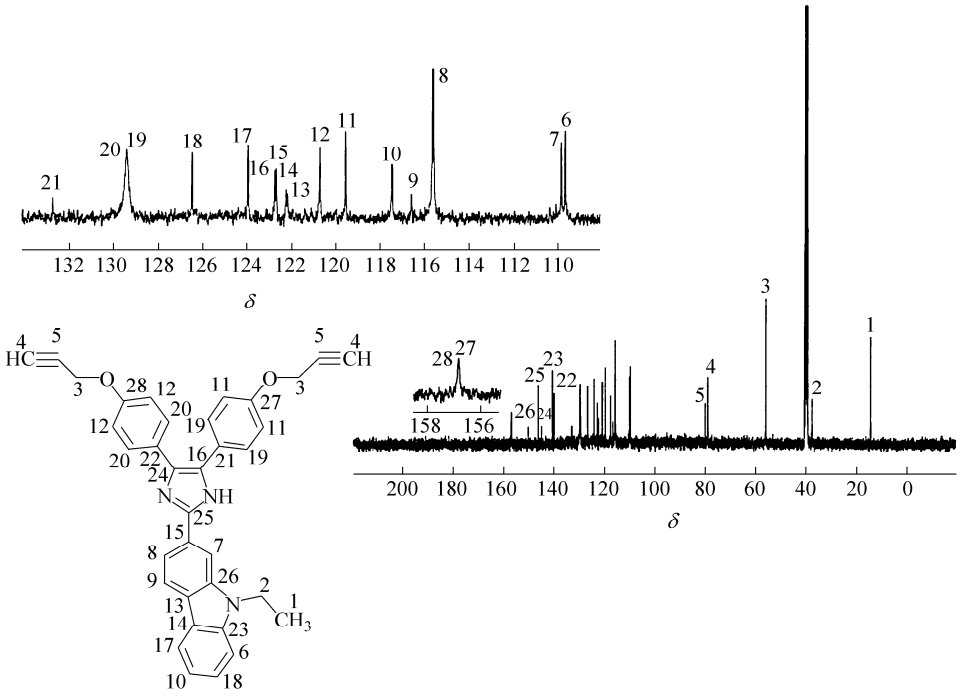

Fig. 3 ^{13}C-NMR spectrum of monomer (**3**) in DMSO-d_6

Synthesis and Characterization of PTAEIs and Nanocomposites

A series of organosoluble high performance polymers PTAEIs bearing functional heterocyclic rings of triazole, imidazole and carbazole in their chains was prepared by the click reaction between a new dialkyne-terminated monomer and several diazide compounds, as shown in Scheme 1. The polymerization reaction proceeded within a homogeneous solution (DMF) in the presence of Cu^{2+} and sodium ascorbate as catalyst. The click reaction was optimized for the preparation of PTAEI8; the highest yield of 91% and inherent viscosity of η_{inh} = 0.59 dL/g were obtained at 60 °C after 24 h. The elemental analysis results were in good agreement with the calculated percentages for carbon, hydrogen and nitrogen contents in PTAEIs repeating units. The weight average

molecular weights (M_w) of these PTAEIs were in the range of 19100–26700 g/mol with distribution index of 1.81–2.07. The results are listed in Table 1. These molecular weights were sufficient to afford flexible and tough thin films by casting the DMF solution of PTAEIs. ^{1}H-NMR spectrum of PTAEI8, in Fig. 4, shows characteristic resonance of triazole at δ = 8.27 (—CH—) and the shift of methylene signal from δ = 4.86 to δ = 5.59. The polymer structure is also confirmed by FTIR spectrum which showed the disappearance of absorption bands corresponding to propargyl (3285 cm^{-1}) and azide (2095 cm^{-1}). PTAEI/GPTES-Fe_3O_4 composites with interfacial adhesion between organic and inorganic phases have been successfully prepared. Fe_3O_4 nanoparticles were first prepared and then activated in methanesulfonic acid for 12 h. In order to improve dispersion of nanoparticles in polymer matrix and enhance the interfacial interaction between the two phases, GPTES molecules were linked to the Fe_3O_4 surface *via* Fe—O—Si bonds. This was achieved by condensation of hydroxyl groups (—OH) on the surface of activated Fe_3O_4 with the hydrolysable methoxy groups (—OCH_3) of GPTES. FTIR spectrum of Fe_3O_4 in Fig. 2 presents absorption bands at 586 cm^{-1} related to Fe—O vibration mode, at 890 cm^{-1} and 790 cm^{-1} due to stretching of Fe–O–H and at 3400 cm^{-1} to the characteristic stretching vibration of hydroxyl group (—OH).

Table 1. Average molecular weights, viscosity and optical properties data of PTAEIs and nanocomposites

Code	η_{inh}[a] (dL/g)	M_w (g/mol)	M_n (g/mol)	Moisture absorption (%)	λ_{ab}[a] (nm)	λ_{em}[a] (nm)	λ_{ab}[b] (nm)	λ_{em}[b] (nm)	Φ_f[a] (%)
PTAEI4	0.44	21300	11200	9.31	316	415	317	419	11
PTAEI5	0.46	23700	13200	9.77	263	422	266	429	19
PTAEI6	0.55	25400	12700	10.43	310	417	311	426	16
PTAEI7	0.41	19100	10000	9.14	310	415	312	420	12
PTAEI8	0.59	26700	13000	12.37	314	416	318	424	14
MNCPTAEI4–10%	–	–	–	10.41	–	–	320	422	–
MNCPTAEI4–30%	–	–	–	10.55	–	–	324	427	–
MNCPTAEI5–10%	–	–	–	10.52	–	–	271	443	–
MNCPTAEI5–30%	–	–	–	10.69	–	–	274	446	–
MNCPTAEI6–10%	–	–	–	11.70	–	–	314	441	–
MNCPTAEI6–30%	–	–	–	11.81	–	–	319	435	–
MNCPTAEI7–10%	–	–	–	10.02	–	–	326	424	–
MNCPTAEI7–30%	–	–	–	10.28	–	–	329	429	–
MNCPTAEI8–10%	–	–	–	12.97	–	–	334	430	–
MNCPTAEI8–30%	–	–	–	13.11	–	–	337	436	–

Polymer concentration for η_{inh} measurement was 0.20 g/dL in NMP.

λ_{ab}[a] and λ_{ab}[b] UV-Visible absorption data of PTAEIs in solutions and in films and nanocomposites in films. λ_{em}[a] and λ_{em}[b] fluorescence emission data of PTAEIs in solutions and in films and nanocomposites in films.

[c] Fluorescence quantum yield was measured relative to quinine sulfate (10^{-5} mol/L, Φ_f = 0.55) in 1 mol/L H_2SO_4 as a standard.

M_w and M_n were measured by GPC at 30 °C using DMF as fluent at 1 mL/min and monodisperse polystyrene for calibration.

FTIR spectrum of GPTES-Fe_3O_4 in Fig. 2 presents a few absorption bands; around 900–1100 cm^{-1} can be assigned to the characteristic vibration bands of Si—O link and epoxide group stretching vibration, at 3400 cm^{-1} to the characteristic stretching vibration of hydroxyl group (—OH) on the surface of Fe_3O_4, at 1380 cm^{-1} to the bending and at 2906–2857 cm^{-1} to the stretching vibrations of C—H of organic methylene. The above interpretations are enough to suggest that GPTES is bound on the surface of Fe_3O_4 particles. Magnetic GPTES-Fe_3O_4/PTAEI nanocomposites (MNCPTAEI) were prepared by solution blending (at 70 °C) *via* interfacial reaction between epoxide-terminated GPTES-Fe_3O_4 and amines of heterocyclic rings in PTAEI chains, as illustrated in Scheme 1.

FTIR spectrum of PTAEI8, in Fig. 2, exhibits the characteristic absorption bands of N—H stretching of imidazole ring at 3300–3400 cm^{-1}, C—N—C stretching at 1375 cm^{-1}, N—H bending at 1619 cm^{-1} and triazole ring stretching at 1580 and 1450 cm^{-1}. FTIR spectrum of nancomposite containing 30 wt% GPTES-Fe_3O_4

exhibits changes in the absorption bands at 1600 cm^{-1} and 3300 cm^{-1} in comparison with the spectrum of PTAEI, Fig. 2. These changes can be due to protonation of tertiary amines and reaction of secondary amine with the epoxide groups of GPTES-Fe_3O_4. Previous studies[18, 35] suggested reaction of tertiary amines of triazole and pyridine with the epoxide groups that might lead to a zwitterionic structure. DSC technique was also used to study the occurrence of reaction between epoxide groups of GPTES-Fe_3O_4 and PTAEI chains. In this regard, mixture of PTAEI4 and GPTES-Fe_3O_4 was heated in the DSC sample pan and, as can be seen in Fig. 5(a), an exothermic peak appeared in the temperature range of 80–100 °C. As can be seen in this figure, the prepared nanocomposites (MNCPTAEI4-10% and MNCPTAEI4-30%), by solution blending at 70 °C, did not show exothermic peak in the region of 100 °C.

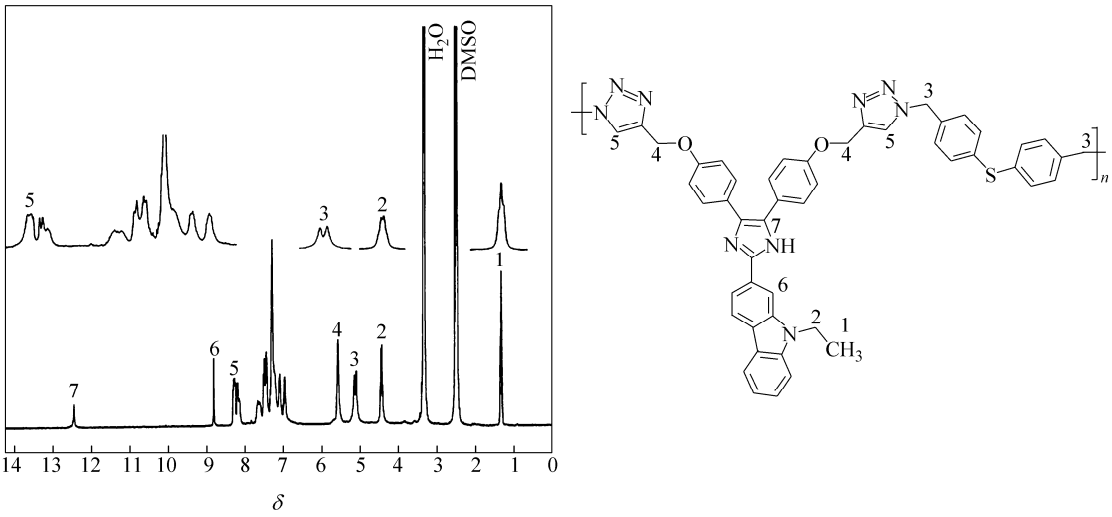

Fig. 4 ^{1}H-NMR spectrum of PTAEI8 in DMSO-d_6

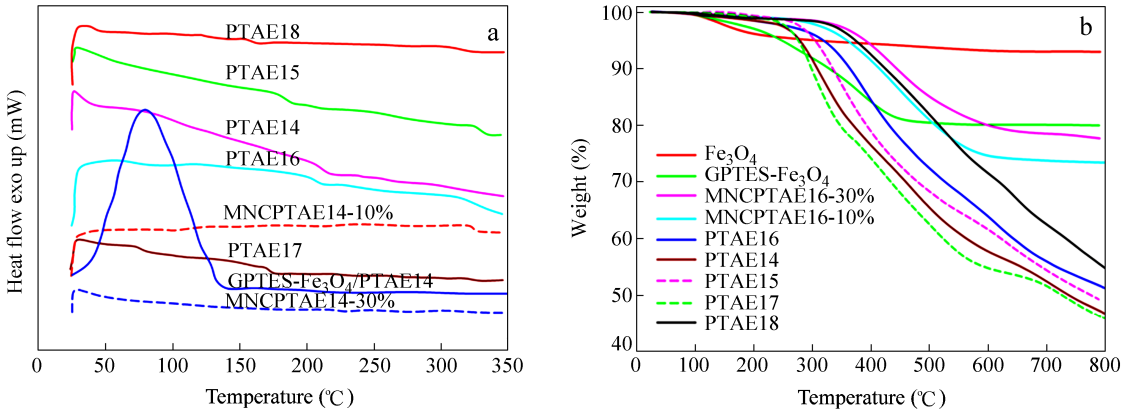

Fig. 5 (a) DSC curves of PTAEIs, nanocomposites and cure curve of GPTES-Fe_3O_4/PTAEI4 mixture; (b) TGA curves of Fe_3O_4, GPTES-Fe_3O_4, PTAEIs and nanocomposites under N_2 at a heating rate of 10 K/min

The absence of exothermic peak for nanocomposites indicates that amines of heterocyclic rings in PTAEI chains reacted with the electron poor methylene of the epoxide ring during preparation of nanocomposite. The above interpretations, and also the insolubility of the nanocomposites in organic solvents, are enough to suggest that GPTES-Fe_3O_4 is interfecially bound with the PTAEI chains. Figure 5(b) shows the TGA curves of Fe_3O_4 and GPTES-Fe_3O_4. It can be seen that the weight loss is 7% in temperature range of 0–200 °C for Fe_3O_4 (almost no weight loss over 300 °C), it is mainly due to the loss of absorbed moisture. The weight of GPTES-Fe_3O_4

decreases quickly over 200 °C and the loss is about 20% over 400 °C, which can be attributed to the thermal decomposition of GPTES at high temperatures. By comparison of the TGA curves in Fig. 5(b), it can be deduced that the maximum mass fraction of GPTES on the surface of Fe_3O_4 is about 20%.

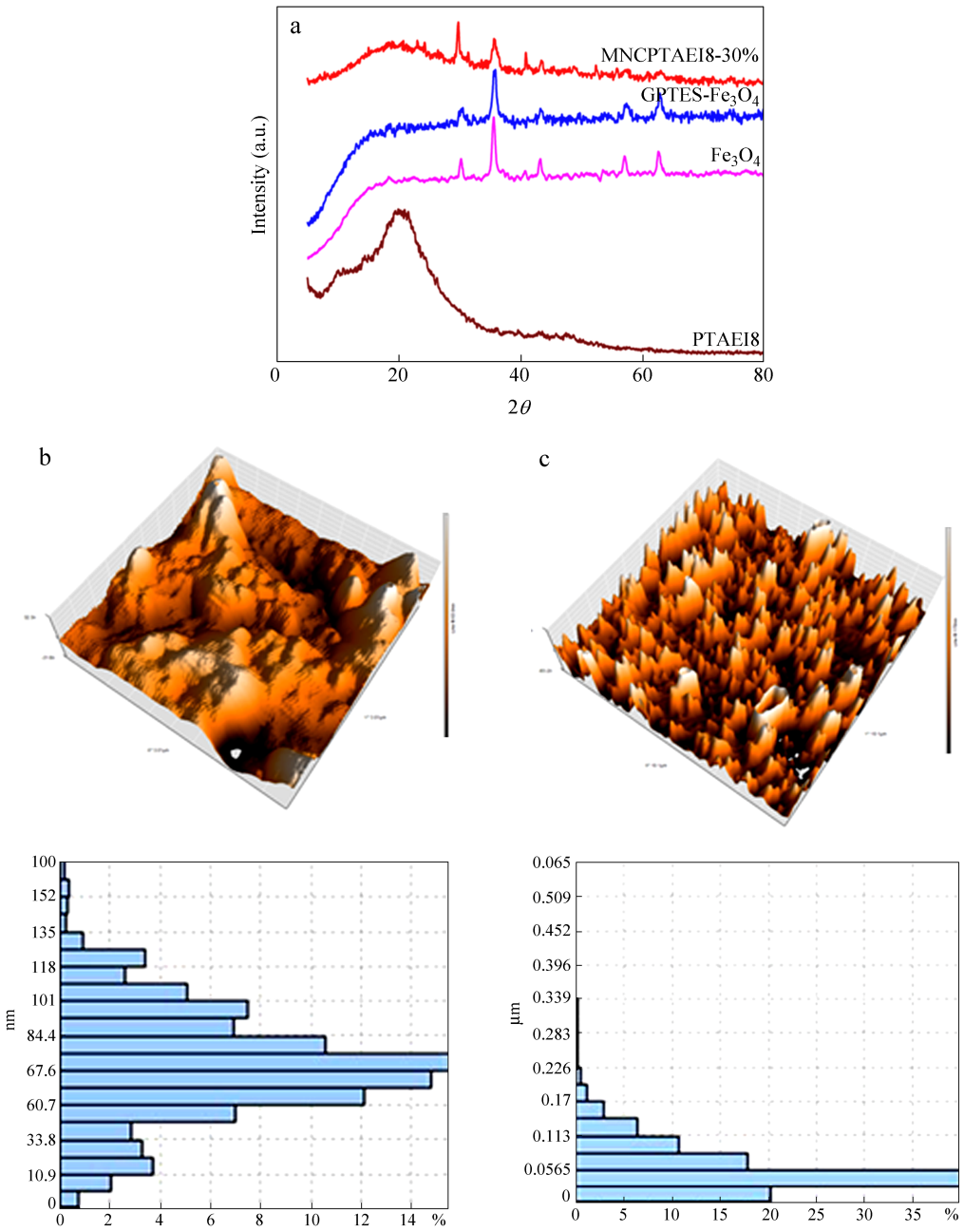

Fig. 6 (a) X-ray diffraction patterns of Fe_3O_4, GPTES-Fe_3O_4, PTAEI8 and nanocomposite; (b) AFM images of GPTES-Fe_3O_4 and (c) nanocomposite

X-ray diffraction (XRD) technique has been used to examine the nature of the nanocomposites with respect to pure PTAEIs. XRD patterns for PTAEI8, GPTES-Fe_3O_4, and MNCPTAEI8-10% are shown in Fig. 6(a). According to XRD patterns, neat PTAEI8 is totally amorphous in nature which does not show any sharp

diffraction peaks, but the composite containing 10 wt% GPTES-Fe_3O_4 expresses that the crystal structure of Fe_3O_4 was not altered due to the presence of PTAEI8. However, the peaks intensity depends on the amount of modified GPTES-Fe_3O_4 in the composite.

Morphology and Dispersibility of GPTES-Fe_3O_4

In order to examine the microstructures and particles distribution within the nanocomposites, FE-SEM and AFM analysis were conducted. Figures 6(b, c) show AFM images of neat Fe_3O_4 and GPTES-Fe_3O_4. The surface roughness with average size of 67.5 nm is observed for Fe_3O_4 particles, while the surface of GPTES-Fe_3O_4 sample is rougher with average size of 56 nm. This change in the size indicates less agglomeration of magnetic nanoparticles after they were surface modified with organosilane coupling agent, GPTES. Typical surface FE-SEM images of Fe_3O_4, GPTES-Fe_3O_4 and magnetic nanocomposite with 10 wt% GPTES-Fe_3O_4 are illustrated in Figs. 7(a–c). In comparison with the neat Fe_3O_4 in Fig. 7(a), it can be observed that the particles size of GPTES-Fe_3O_4, Fig. 7(b), decreased due to less aggregation as a result of surface coating, while the composite image in Fig. 7(c) shows particles size increased which can be due to presence of nanoparticles in the polymer matrix. TEM micrograph of the hybrid film in Fig. 7(d) shows dispersion of GPTES-Fe_3O_4 particles in the polymer matrix and reveals the core-shell structure.

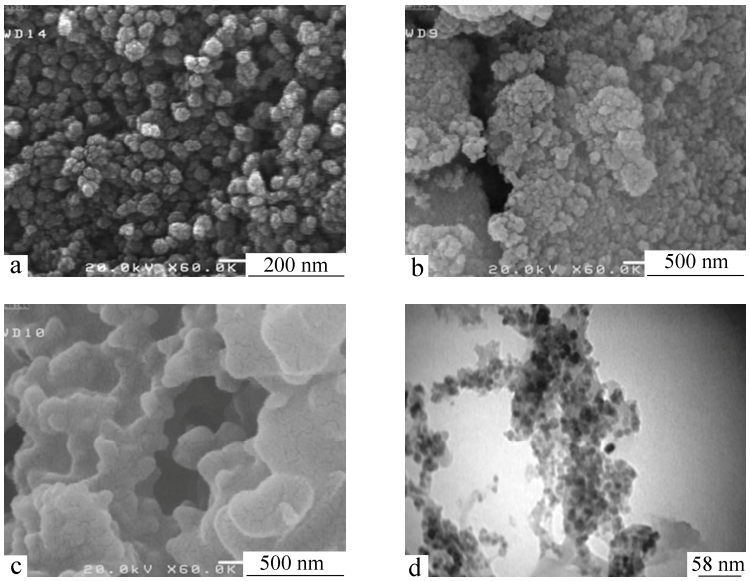

Fig. 7 FE-SEM images of (a) Fe_3O_4, (b) GPTES-Fe_3O_4, (c) MNCPTAEI8-10% and (d) TEM image of MNCPTAEI8-30%

Properties of PTAEIs and Nanocomposites

Solubility and moisture absorption

As a general rule, high solubility is a desired prerequisite for polymer processing. The solubility behavior of PTAEIs and nanocomposites was tested qualitatively in various organic solvents. All PTAEIs exhibited excellent solubility in polar aprotic solvents such as NMP, DMAc, DMF, DMSO and even in less polar solvents like pyridine and THF. The good solubility of these polymers should be governed by incorporation of several factors such as ether linkage, heterocyclic triazole and imidazole rings and packing-disruptive bulky carbazole which increased chain-packing distances and decreased inter-chain interactions resulting in amorphous polymers. These factors contributed to the enhanced solubility of these polymers through better penetration of solvent molecules and formation of H-bonding with the polar sites in the polymer chains. However, nanocomposites did not show any solubility in these solvents. These results also reveal that PTAEI and GPTES-Fe_3O_4 have definitely been involved in formation of structural network via interfacial reactions between epoxide groups of GPTES-Fe_3O_4 and amines of heterocyclic rings. The moisture absorption influences the final application of high performance

materials. The absorbed water diminishes T_g and influences mechanical and electrical properties, but in membrane technology, greater water uptake implied better performance. The obtained results for the moisture absorption were in the range of 9.14%–13.11%. The relatively high percent of moisture absorption corresponds to the presence of hydrophilic functional groups in the PTAEIs chains. In general, the loose packing of PTAEIs chains due to bulky pendant results in the increase of free volume that should ensure the polymer to entrap some of the water molecules.

Photophysical properties

The photophysical properties of PTAEIs and nanocomposites were investigated by UV-Vis and fluorescence spectroscopy. The dilute solution of PTAEI in DMF (0.2 g/dL) and films of nanocomposites (thickness ~1 mm) showed strong UV absorption with maximum at λ_{ab} = 266–337 nm indicating a relatively small energy band gap for π/π^* transition. This can be attributed to the aromatic moieties in the PTAEIs backbone. To investigate the fluorescence emission properties, an excitation wavelength of 320 nm was used in all cases. The fluorescence emission spectra of PTAEIs in dilute solutions and also for nanocomposite films are shown in Fig. 8. To measure the photoluminescence (PL) quantum yields (Φ_f), dilute PTAEIs solutions (0.2 g/dL) in DMF were prepared. A 0.10 N solution of quinine in H_2SO_4 (Φ_f = 0.53) was used as a reference[36]. The solution and thin films of PTAEIs emitted fluorescence light in blue and green color with the maximum wavelengths in the range of λ_{em} = 415–430 nm and Φ_f = 11%–19%, as listed in Table 1. As shown in the left corner in Fig. 8, PTAEI5 showed more intense fluorescence emission and higher quantum yield (Φ_f = 19%) in comparison with other PTAEIs which can be due to presence of anthracene in the backbone of this polymer. In comparison with the spectra of neat PTAEIs, the fluorescence emission spectra of the nanocomposite films containing 10 wt% and 30 wt% GPTES-Fe_3O_4 have shifted towards higher wavelength, as shown in Fig. 8.

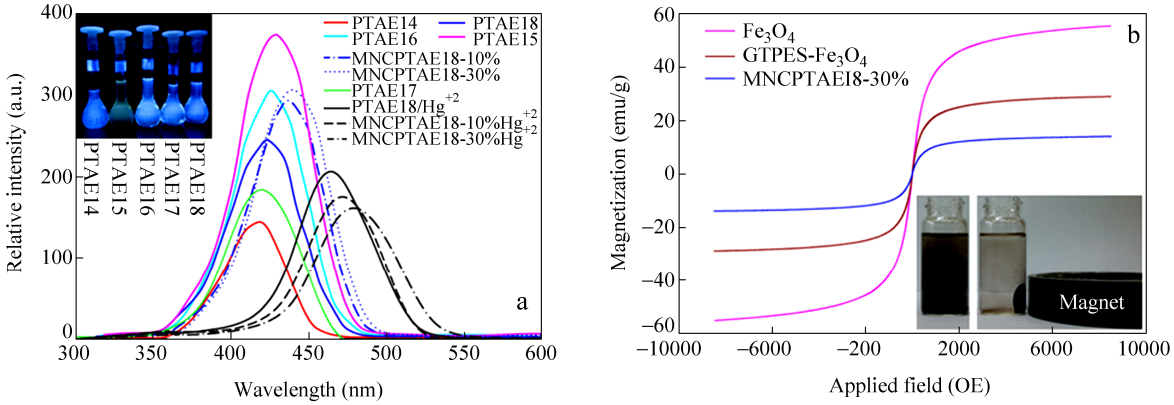

Fig. 8 (a) Fluorescence spectra of PTAEI, nanocomposites and complex of nanocomposite with Hg^{+2}; (b) VSM images of Fe_3O_4, GPTES-Fe_3O_4 and nanocomposite.

Mechanical properties

The tensile stress-strain curve is a tool to provide data on toughness (area under the curve), ultimate tensile strength, ultimate elongation at break and Young's modulus. The mechanical properties of PTAEIs and nanocomposites were measured in the tensile mode and the results are summarized in Table 2. An average of five individual measurements was used for each sample. PTAEIs showed tensile strength in the range of 69–108 MPa with elongation to break of 8.99%–13.76% and Young's modulus (E) of 1.70–2.26 GPa. Among the prepared PTAEIs, PTAEI5 with anthracene ring in the repeating unit showed the highest tensile strength of 108 MPa. As can be seen in Table 2, the tensile strength of PTAEIs increased with the addition of GPTES-Fe_3O_4; and simultaneously, the tensile elongation at break decreased. The tensile strength has increased from 91 MPa for neat PTAEI7 to 119 MPa and 134 MPa for composite containing 10 wt% and 30 wt % GPTES-Fe_3O_4, and elongation at break decreased from 11.4% to 10.3% and 9.2%, respectively. The enhancement of

tensile strength corresponds to the forecast that Fe_3O_4 could play a reinforcing role in the composite. It might be ascribed to the fine dispersion of GPTES-Fe_3O_4 in the polymer matrix and formation of strong interfacial interactions between inorganic and organic phases. These factors can lead to the efficient load transfer from polymer matrix to nanoparticles and less stress convergence during the elongation process.

Analysis of magnetic properties

Vibrating sample magnetometry (VSM) was employed to study the magnetic properties of the prepared Fe_3O_4, GPTES-Fe_3O_4 and composites. The magnetic hysteresis loops of these materials were determined as a function of applied magnetic field at room temperatures and the results are illustrated in Fig. 8(b). It is vitally important that materials which are suggested for the sorbents should possess sufficient magnetic and superparamagnetic properties. As can be seen, naked Fe_3O_4 nanoparticles have high saturation magnetization of 58 emu/g at 8000 Oe, with remanence and coercivity of zero in the absence of external magnetic field. The very weak hysteresis confirms that these materials have superparamagnetic properties at room temperature, which implies that the sample keeps no remanence in the absence of an external magnetic field. The saturation magnetization value for GPTES-Fe_3O_4 and for composite with 30 wt% GPTES-Fe_3O_4 was 29 emu·g^{-1} and 17 emu·g^{-1}, respectively. Compared to the naked Fe_3O_4 (58 emu/g), decrease in the magnetic strength of GPTES-Fe_3O_4 and composite can be due to surface coating of Fe_3O_4 with GPTES and PTAEI chains. However, the saturation magnetization is sufficiently enough which makes the composite very susceptible to magnetic fields and separation from a suspension can proceed easily and quickly with a conventional magnet, as shown in Fig. 8(b). The magnetic properties (saturation magnetization and superparamagnetic behavior) of the present polymer-based nanoparticles can also be of interest for drug targeting purposes and also for bioapplications, such as magnetic resonance imaging (MRI) agents, where M_s of 7–22 emu/g is usually needed[37].

Table 2. Thermal and mechanical properties of PTAEIs and nanocomposites

Code	Tensile strength (MPa)	Tensile Modulus (GPa)	Elongation at break (%)	T_g [a] (^oC)	$T_{10\%}$ [b] (^oC)	C.Y.[c]	LOI [d] (%)
PTAEI4	69 ± 2	1.70 ± 0.14	10.4 ± 1.6	211	308	46	36
PTAEI5	108 ± 4	2.26 ± 0.07	9.0 ± 0.09	184	334	49	37
PTAEI6	83 ± 1	1.96 ± 0.11	13.7 ± 1.4	207	369	51	38
PTAEI7	91 ± 2	1.89 ± 0.09	11.4 ± 1.3	171	301	45	36
PTAEI8	99 ± 3	1.97 ± 0.18	17.1 ± 1.7	160	426	55	40
MNCPTAEI4-10%	75 ± 2	1.77 ± 0.07	7.7 ± 1.1	323	339	77	48
MNCPTAEI4-30%	78 ± 4	1.79 ± 0.10	6.1 ± 1.3	–	353	79	49
MNCPTAEI5-10%	–	–	–	259	370	78	49
MNCPTAEI5-30%	–	–	–	–	389	80	50
MNCPTAEI6-10%	–	–	–	–	417	80	50
MNCPTAEI6-30%	–	–	–	–	445	82	50
MNCPTAEI7-10%	119 ± 5	2.49 ± 0.05	10.3 ± 1.2	234	368	73	47
MNCPTAEI7-30%	134 ± 3	2.54 ± 0.11	9.2 ± 1.4	–	391	77	48
MNCPTAEI8-10%	–	–	–	–	443	81	50
MNCPTAEI8-30%	–	–	–	–	469	84	51

[a] T_g was recorded by DSC at 10 K/min in N_2;
[b] $T_{10\%}$ was recorded by TGA at 10 K/min in N_2;
[c] C.Y. = Char yield, weight% of material left at 800 °C in N_2;
[d] Limiting oxygen index (%) evaluated at char yield 800 °C.

Thermal properties

TGA and DSC methods were applied to evaluate thermal properties of PTAEIs and nanocomposites. Figure 5(a) shows DSC curves of PTAIEs and nanocomposites at 10 K/min under N_2. As can be seen in Fig. 5(a), nanocomposites (MNCPTAEI4-10% and MNCPTAEI4-30%) did not show exothermic peak in the temperature range of 80–100 °C, which proves that epoxide groups of GPTES-Fe_3O_4 were consumed during preparation of composites. The T_g values were recorded at the middle of the transition in the second heating scan after cooling from 350 °C to room temperature, and the results were in the range of 160–211 °C, Table 2. Neither

crystallization exothermic nor melting endotherm was observed by DSC in the range of 25–350 °C, so that PTAEIs were considered to be essentially amorphous. The amorphous nature of these polymers can be attributed to their bulky pendant group which decreased the inter-chain interaction resulting in loose polymer chain packaging and aggregates. In general, molecular packing and chain rigidity are among the main factors influencing T_g values and thermal stability of polymers. Therefore, the increased rotational barrier caused by the bulky pendant enhances T_g value, while T_g value also depends on the stiffness of the existing linkages in the repeating unit. The presence of flexible linkages such as ether, methylene and sulfide in compound (**3**) and in the diazide compounds have reduced T_g values of these polymers in comparison with the T_g of conventional aramids, polyimides and previously reported polymers[38]. In these series of polymers, PTAEI8 showed the lowest T_g value of 160 °C and PTAEI4 exhibited the highest T_g of 211 °C due to better packing and stronger inter-chain interaction. The T_g values of composites showed dependence on the content of GPTES-Fe_3O_4. As shown in Fig. 5(a), PTAEI4 containing 30 wt% GPTES-Fe_3O_4 did not show T_g up to 350 °C, while T_g of PTAEI5 and PTAEI7 increased from 184 °C to 259 °C and from 171 °C to 234 °C when these polymers contained 10 wt% GPTES-Fe_3O_4. Thermal stability of PTAEIs and nanocomposites was evaluated by TGA at a heating rate of 10 K/min under N_2, the results are shown in Fig. 5(b). The corresponding data of 10% weight loss temperatures ($T_{10\%}$), char yields (CR) and limiting oxygen indexes (LOI) calculated based on the char yields at 800 °C are listed in Table 2. CR values can be used as criteria for evaluating LOI of polymers in accordance with Van Krevelen and Hoftyzer equation[39], LOI = 17.5 + 0.4CR. In general, when LOI value of a polymer is higher than 26% it is considered to be inflammable. The $T_{10\%}$ values for PTAEIs stayed within 301–426 °C, depending on the chemical structure of the repeating unit. Among these polymers, PTAEI8 with sulfide linkage in the repeating unit showed the highest thermal stability with $T_{10\%}$ = 426 °C. Figure 5(b) also shows TGA curves of the representative nanocomposites containing 10 wt% and 30 wt% GPTES-Fe_3O_4. The $T_{10\%}$ values increased from 301–426 °C for the neat PTAEIs to 353–469 °C for the composites containing 30 wt% GPTES-Fe_3O_4. As shown in Table 2, $T_{10\%}$ value of PTAEI6 increased from 369 °C to 417 °C and 445 °C when contained 10 wt% and 30 wt% GPTES-Fe_3O_4, respectively. It is clear that good dispersion of surface modified Fe_3O_4 in the polymer matrix and strong interfacial interaction have also enhanced thermal stability of the nanocomposites.

Extraction of metal cations from aqueous solutions

As PTAEIs have many chelating sites in their chains such as triazole and imidazole rings and are insoluble in water, therefore, solid-liquid extractions have been carried out with PTAEI8 and magnetic nanocomposite containing 30 wt% GPTES-Fe_3O_4. Extraction of Cr^{3+}, Pb^{2+}, Cd^{2+}, Sn^{2+}, Cu^{2+} and Hg^{2+} ions as their nitrate salts was carried out at pH = 7 from aqueous solutions either individually or in the mixture. The amount of adsorbed ions was calculated using the following equation, (Eq. 1):

$$Q_t = \frac{[(c_0 - c_A) \times V]}{w} \tag{1}$$

where Q_t is the amount of metal ion adsorbed into the unit of the composite ($mg \cdot g^{-1}$), c_0 and c_A are concentration ($mg \cdot mL^{-1}$) of metal ions in the initial solution and in the aqueous phase after adsorption, respectively, V is the volume of the initial solution (mL) and w is the weight of the adsorbent (g). The efficiency for ion adsorption from the solution R (%) was calculated using the following equation:

$$R = (c_i - c_e)/c_i \times 100 \tag{2}$$

where c_i and c_e is concentration of ions in the initial solution and at the equilibrium, respectively. Selectivity coefficient of adsorption of metal ions in the solution was studied in the mixture by batch procedure. The distribution coefficients (k_d) of ions were determined by the following equation, (Eq. 3):

$$K_d = \frac{[(c_0 - c_A) \times V]}{c_A \times w} \tag{3}$$

The extraction selectivity, α, is the ratio of two distribution coefficients as shown in equation (4). The Hg^{2+} cation was taken as the reference, as it has the highest distribution coefficient.

$$\alpha = \frac{K_{d M^{n+}}}{K_{d Hg^{2+}}} \tag{4}$$

The results for distribution coefficient and selectivity in the mixture of metal ions in solution are shown in Table 3. As can be seen in this table, the extraction level of these cations Cr^{3+}, Pb^{2+}, Cd^{2+}, Sn^{2+}, Cu^{2+} and Hg^{2+} by the nanocomposite increased in comparison with the absorption level by neat PTAEI8. Also, the selective adsorption of Hg^{2+} cation in the mixture solution of all cations is the highest which is similar to the results obtained for each ion individually. It is clear from the selectivity factor, that the quantitative separation of Hg^{2+} cation from the rest of the cations is possible. The photoluminescence (PL) property of PTAEI8-Hg^{2+} and nanocomposite-Hg^{2+} complexes was investigated by fluorescence spectroscopy. As can be seen in Fig. 8(a), PTAEI8 exhibited pronounced fluorescence response after adsorption of Hg^{2+} ions, the emission intensity decreased and the maximum shifted from 425 nm for the neat PTAEI8 to 465 nm for PTAEI8-Hg^{2+} complex. The responsive optical property is also the same for nanocomposite-Hg^{2+} complex. The decrease in the emission intensity can be due to quenching of the excited chromophore groups by complex formation with Hg^{2+} ions. The results indicate that these conjugated polymers with triazole units in the chains can be used as a selective fluorescence sensor for Hg^{2+} detection. The extraction level of the tested metals especially mercury from aqueous media points to future applications of PTAEIs and their magnetic nanocomposites in the field of membrane preparation for cation transport, water decontamination and in sensing materials, among other applications.

Table 3. Distribution coefficient (K_d), efficiency of ions adsorption R (%) and selectivity factor (α) in competitive extraction conditions

	PTAEI8		
Metal Cation	Distribution coefficient (K_d, mL·g^{-1})	R (%)	Selectivity factor (α)
$Hg(NO_3)_2$	5305.56	95.5	1.00
$Cd(NO_3)_2$	1546.88	86.1	0.29
$Cu(NO_3)_2$	893.14	78.1	0.17
$Pb(NO_3)_2$	402.03	61.7	0.08
$Cr(NO_3)_3$	3881.92	93.9	0.73
$Sn(NO_3)_3$	311.62	55.5	0.06
	MNCPTAEI8-30%		
$Hg(NO_3)_2$	9365.38	97.4	1.00
$Cd(NO_3)_2$	3128.38	92.6	0.33
$Cu(NO_3)_2$	1058.91	80.9	0.11
$Pb(NO_3)_2$	766.26	75.4	0.08
$Cr(NO_3)_3$	6892.86	96.5	0.74
$Sn(NO_3)_3$	750.01	75.0	0.08

CONCLUSIONS

The design and synthesis of novel high performance polymers with improved solubility based on combined heterocyclic rings of triazole, imidazole and carbazole was the main objective of this work. Therefore, a dialkyne-terminated compound was synthesized, characterized and used in copper-catalyzed click polymerization with several diazides. The obtained organosoluble polymers, poly(triazole-ether-imidazole)s PTAEIs, with M_w = 19100–26700 g/mol exhibited good film-forming capability, relatively high fluorescence emission, reasonable thermal stability (T_g = 160–211 °C and $T_{10\%}$ = 301–426 °C) and mechanical properties suitable for thermoforming processing. These PTAEIs with functional heterocyclic moieties in the backbone were used in the preparation of chemically bonded reinforced composite materials with the surface modified magnetic Fe_3O_4. As compared with the pure PTAEIs, the GPTES-Fe_3O_4/PTAEIs nanocomposites are significantly strengthened by increasing the tensile strength and have an improved thermal stability. The results

also demonstrated that these PTAEIs and particularly their composites with GPTES-Fe_3O_4 can act efficiently as chelating agent for heavy metal ions. This strategy offers notable versatility, opening the avenue for the facile fabrication of multifunctional polymers and hybrid compounds.

REFERENCES

1 Tornoe, C.W., Christensen, C. and Meldal, M., J. Org. Chem., 2002, 67: 3057
2 Rostovtsev, V.V., Green, L.G., Fokin, V.V. and Sharpless, K.B., Angew. Chem., 2002, 114: 2708
3 Bock, V.D., Hiemstra, H. and Van Maarseveen, J.H., Eur. J. Org. Chem., 2006, 2006: 51
4 Li, H.K., Sun, J.Z., Qin, A.J. and Tang, B.Z., Chinese J. Polym. Sci., 2012, 30(1): 1
5 Meldal, M. and Tornøe, C.W., Chem. Rev., 2008, 108: 2952
6 Hein, J.E. and Fokin, V.V., Chem. Soc. Rev., 2010, 39: 1302
7 Hsiao, S.H., Liou, G.S., Kung, Y.C. and Lee, Y.J., Eur. Polym. J., 2010, 46: 1355
8 Garcıa, J.M., Garcıa, F.C., Serna, F. and de la Pena, J.L., Prog. Polym. Sci., 2010, 35: 623
9 Liaw, D.J., Hsu, P.N., Chen, W.H. and Lin, S.L., Macromolecules, 2002, 35: 4669
10 Yue, K., He, J., Liu, C., Huang, M., Dong, X.H., Guo, K., Ni, P., Wesdemiotis, C., Quirk, R.P., Cheng, S.Z.D. and Zhang, W.B., Chinese J. Polym. Sci., 2013, 31(1): 71
11 Hsiao, S.H., Chen, C.W. and Liou, G.S., J. Polym. Sci., Part A: Polym. Chem., 2004, 42: 3302
12 Ghaemy, M., Nasr, F.H., Alizadeh, R. and Taghavi, M., Macromol. Res., 2012, 20: 614
13 Ghaemy, M., Aghakhani, B., Taghavi, M., Amini Nasab, S.M. and Mohseni, M., React. Funct. Polym., 2013, 73: 555
14 Ghaemy, M., Qasemi, S., Ghassemi, K. and Bazzar, M., J. Polym. Res., 2013, 20: 278
15 Raj, V., Madheswari, D. and Ali, M.M., J. Appl. Polym. Sci., 2011, 119: 2824
16 Liou, G.S., Hsiao, S.H., Huang, N.K. and Yang, Y.L., Macromolecules, 2006, 39: 5337
17 Ghaemy, M., Hassanzadeh, M., Taghavi, M. and Amini Nasab, S.M., J. Fluorine. Chem., 2012, 142: 29
18 Bazzar, M., Ghaemy, M. and Alizadeh, R., React. Funct. Polym., 2013, 73: 492
19 Gómez-Valdemoro, A., San-José, N., Garcia, F.C., De La Pena, J.L., Serna, F. and Garcia, J.M., Polym. Chem., 2010, 1: 1291
20 Uzun, L., Kara, A., Osman, B., Yilmaz, E., Besirli, N. and Denizli, A., J. Appl. Polym. Sci., 2009, 114: 2246
21 Kumar, A. and Pandey, P.S., Tetrahedron Lett., 2009, 50: 5842
22 Chang, K.C., Su, I.H., Senthilvelan, A. and Chung, W.S., Org. Lett., 2007, 9: 3363
23 Zou, H., Wu, S. and Shen, J., Chem. Rev., 2008, 108: 3893
24 Agag, T., Koga, T. and Takeichi, T., Polymer, 2001, 42: 3399
25 Kango, S., Kalia, S., Celli, A., Njuguna, J., Habibi, Y. and Kuma, R., Prog. Polym. Sci., 2013, 38: 1232
26 Ouerghui, A., Elamari, H., Ghammouri, S., Slimi, R., Meganem, F. and Girard, C., React. Funct. Polym., 2014, 74: 37
27 Hu, J., Irene, M.C. and Chen, G., Langmuir, 2005, 21: 11173
28 Rahmani, A., Zavvar Mousavi, H. and Fazli, M., Desalination, 2010, 253: 94
29 Liu, J.F., Zhao, Z.S. and Jiang, G.B., Environ. Sci. Technol., 2007, 42: 6949
30 Tian, Y., Shi, W., Luo, J., Ma, F., Mi, H. and Lei, Y., J. Polym. Sci., Part A: Polym. Chem., 2013, 51: 3636
31 Taghavi, M., Ghaemy, M., Amini Nasab, S.M. and Hassanzadeh, M., Polymer, 2013, 54: 3828
32 Wu, Y.C. and Kuo, S.W., Polymer, 2010, 51: 3948
33 Yao, S.H., Ahn, Y., Wang, X., Fu, J., Van Stryland, E.W., Hagan, D.J. and Belfield, K.D., J. Org. Chem., 2010, 75: 3965
34 Seckin, T., Vural, S. and Koytepe, S., Polym. Bull., 2010, 64: 115
35 Ryu, B.Y. and Emrick, T., Macromolecules, 2011, 44: 5693
36 Liou, G.S. and Chang, C.W., Macromolecules, 2008, 41: 1667
37 Li, M., Xu, L.Q., Wang, L., Wu, Y.P., Li, J., Neoh, K.G. and Kang, E.T., Polym. Chem., 2011, 2: 1312
38 Ghaemy, M., Hassanzadeh, M., Amini Nasab, S. M. and Taghavi, M., Polym. J., 2013, 45: 622
39 Van Krevelen, D.W. and Hoftyzer, P.J. Properties of Polymers, 4rd ed., Amsterdam, Elsevier Scientic Publishing, 2008